Soft Matter

www.softmatter.org

Volume 5 | Number 9 | 7 May 2009 | Pages 1745–1948

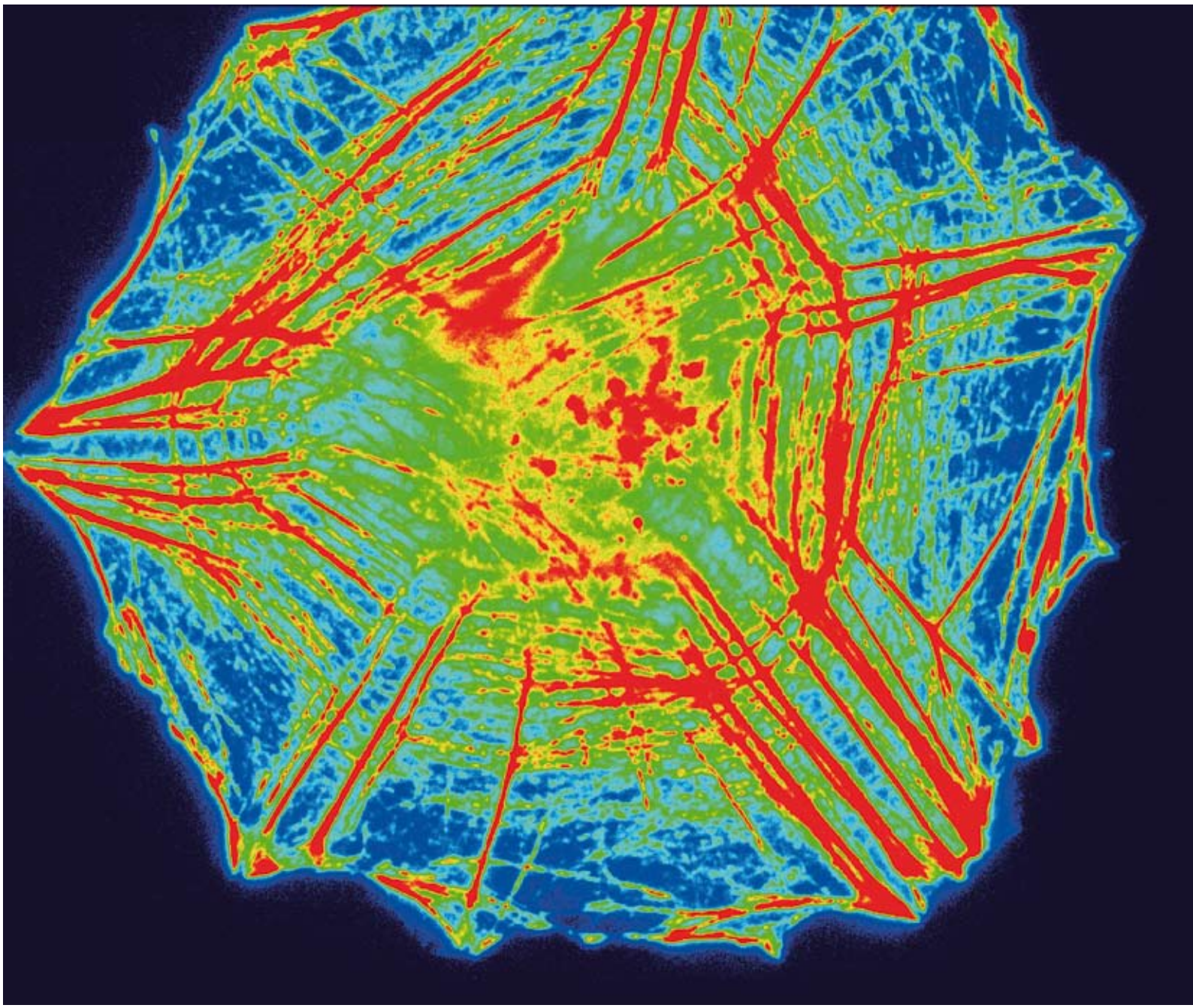

ISSN 1744-683X

RSC Publishing

PAPER
Andreas Bausch *et al.*,
Structural polymorphism in heterogeneous cytoskeletal networks

HIGHLIGHT
Manuel Laso and Martin Kröger *et al.*
Random packing of model polymers: local structure, topological hindrance and universal scaling

1744-683X(2009)5:9;1-D

Structural polymorphism in heterogeneous cytoskeletal networks†

Oliver Lieleg,[a] Kurt M. Schmoller,[a] Christian J. Cyron,[b] Yuxia Luan,[ac] Wolfgang A. Wall[b] and Andreas R. Bausch*[a]

Received 20th August 2008, Accepted 12th December 2008
First published as an Advance Article on the web 6th February 2009
DOI: 10.1039/b814555p

The viscoelastic response of living cells is largely determined by heterogenous networks of cross-linked and bundled actin filaments. The quantitative impact of such local network heterogeneities is studied best in well-defined *in vitro* model systems by employing microscopic and micromechanical techniques. In this study, we show that reconstituted α-actinin/actin networks exhibit a structural polymorphism, which is dictated by two types of mesoscopic heterogeneities: a composite bundle phase at intermediate α-actinin concentrations and clusters of actin bundles at high α-actinin concentrations. We demonstrate the influence of these structural heterogeneities on the mechanical properties of cross-linked and bundled actin networks. First, locally embedding stiff bundles into the network strengthens the macroscopic network response. Second, the formation of fractal, star-like bundle clusters drastically concentrates material in localized spots and weakens the network elasticity. Such bundle cluster networks exhibit kinetically trapped and thus metastable network configurations—which is contrary to the commonly accepted belief of equilibrated network formations.

Introduction

Cells make use of semi-flexible polymers to form networks that provide structural integrity and can withstand mechanical load. The mechanical properties of the cytoskeleton are mainly attributed to the biopolymer actin.[1,2] To obtain a physical understanding regarding the formation and the mechanical function of cytoskeletal networks, a bottom-up approach has been proven essential since the microstructure of reconstituted systems can be controlled.[3] Above the overlap concentration actin filaments form entangled solutions that are mechanically weak. Actin binding proteins (ABPs) can significantly enhance the elasticity of an entangled actin solution; their effectiveness in increasing the elasticity sensitively depends on their micro-mechanical and biochemical properties[4–7] and on their effect on the network microstructure.[8–10] α-Actinin belongs to a highly conserved family of ABPs; its different isoforms are ubiquitous in muscle as well as in non-muscle cells.[11] In the latter, α-actinin is predominantly found to form stiff contractile bundles—so called 'stress-fibers'.[12] These bundles are embedded into a filamentous actin network. It was shown that α-actinin can also bundle actin filaments *in vitro*.[13,14] Yet, the resulting network morphology seems to strongly depend on the α-actinin concentration as different network structures have been reported. Although a homogenous network of bundles has been observed at high α-actinin concentrations,[15] also intrinsically heterogeneous networks have been described: composite networks have been seen at lower concentrations[13] and at very low concentrations the appearance of microdomains has been proposed.[16] While homogeneous phases seem to be the result of free energy minimizations,[3,17] a clear classification and characterization of heterogeneous actin networks is missing. So far, a detailed quantitative physical description of the viscoelastic properties of actin networks has been achieved for pure systems with well-defined microstructures, *e.g.* networks consisting of either single filaments or bundles only.[8,10] For such isotropically cross-linked or homogeneous bundle networks, the microscopic origin of the network elasticity has been identified.[8,10,18,19] These homogeneous networks are relatively simple and exhibit only two different structural and mechanical phases.[10,20] In order to achieve significant progress in the understanding of heterogeneities in cytoskeletal networks, a systematic identification of the structural polymorphism as well as a characterization of the resulting viscoelastic network properties is crucial. Only an integrated approach combining micro- and macrorheological techniques with optical microscopy and simulations can provide the basis for a detailed understanding of the mechanical properties of such heterogeneous cytoskeletal networks.

Here, we demonstrate that the structural polymorphism of reconstituted α-actinin/actin networks goes beyond the equilibrium phases described until now. We identify two types of structural heterogeneities in these networks and elucidate their influence on the macroscopic network response. First, locally embedding stiff bundles into the network efficiently strengthens the macroscopic network response while the local network elasticity remains low. Second, the formation of star-like clusters drastically concentrates material in localized spots. Using finite element simulations, we demonstrate that this rearrangement of bundles into local clusters weakens the overall network elasticity and is responsible for the less effective enhancement of the network elasticity at high α-actinin concentrations. Moreover, in this regime the networks appear to be trapped in a metastable state. This structural phase seems to be the result of a subtle

[a]*Lehrstuhl für Zellbiophysik E27, Technische Universität München, 85748 Garching, GermanyJames-Franck-Straße 1. E-mail: abausch@ph.tum.de*
[b]*Lehrstuhl für Numerische Mechanik, Technische Universität München, 85748 Garching, Germany*
[c]*School of Pharmacy, Shandong University, Jinan, P. R. China*
† Electronic supplementary information (ESI) available. Additional data and pictures as described in the main text. See DOI: 10.1039/b814555p

interplay of growth and aggregation processes since the bundle clusters show a fractal dimension of $d \approx 1.8$.

Results

By increasing the relative α-actinin concentration from $R = \frac{c_{a-\mathrm{act}}}{c_a} = 0$ up to $R = 0.5$, the macroscopic elastic response of α-actinin/actin networks can be enhanced by more than 3 orders of magnitude (see inset of Fig. 1). However, this enhancement is not uniform throughout the whole concentration regime; with respect to R, the plateau modulus G_0—which in this study is approximated by $G'(10\ \mathrm{mHz})$—reveals three distinct regimes as visualized by the three lines of different steepness in Fig. 1. At low α-actinin concentrations, the network elasticity depends only weakly on R. However, above a critical concentration of $R^* \approx 0.01$, a strong increase in the plateau modulus is observed. This regime at intermediate α-actinin concentrations crosses over to a third regime at $R^{\#} \approx 0.1$. Here, the plateau modulus still increases with respect to R; however, the observed enhancement of the network elasticity is weaker than before.

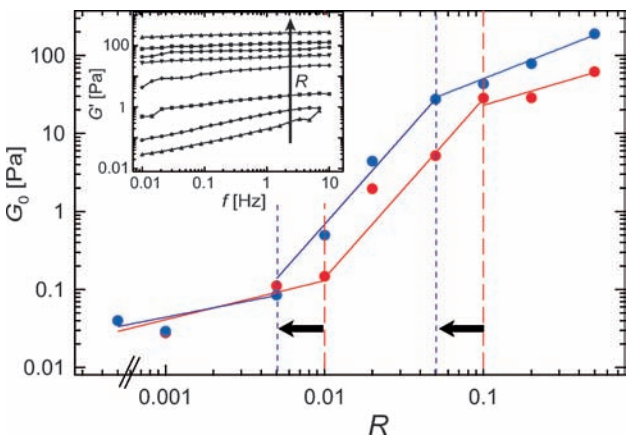

Fig. 1 Plateau elasticity G_0 as a function of the relative α-actinin concentration, R ($c_a = 9.5\ \mu\mathrm{M}$). Three distinct mechanical regimes are observed, the transition points between these regimes can be shifted by temperature as indicated by the dashed lines (red symbols and lines: 18 °C, blue symbols and lines: 12 °C). The inset shows frequency spectra as obtained for α-actinin/actin networks at 12 °C.

The elastic response of α-actinin/actin networks depends sensitively on temperature.[16] This can be rationalized since in general the binding affinity of ABPs towards actin is temperature dependent. The data discussed so far was obtained at 18 °C where the binding affinity of α-actinin is low; at lower temperature the effective amount of bound α-actinin molecules should be increased. As a consequence, the mechanical transition points discussed before should be shifted to lower nominal R-values. Indeed, our data is consistent with such a behavior: Both mechanical transitions, R^* and $R^{\#}$ occur at lower α-actinin concentrations if the network is probed at 12 °C. Note that only the bounderies of the three mechanical regimes are shifted by the temperature change (Fig. 1).

The particular strong or weak dependence of the plateau elasticity on the cross-linker concentration reflects various microscopic information about the probed network. Besides the length-dependent bending stiffness of the constituting bundles[14] and the microscopic deformation mode,[9,10,18,19] the static network elasticity of cross-linked and bundled actin networks is mainly dictated by the microstructure. Therefore, the existence of three distinct mechanical regimes implicates that different network microstructures are present at low ($R < R^*$), intermediate ($R^* < R < R^{\#}$) and high ($R > R^{\#}$) α-actinin concentrations.

1. Weakly cross-linked phase

The weak dependence of the plateau modulus on the α-actinin concentration that is observed in the first regime below R^* is generic for all kinds of ABPs[4,10] and even low levels of depletion forces.[21] This weakly cross-linked regime has already been studied in great detail for actin networks cross-linked by the myosin fragment HMM (heavy meromyosin) in the rigor state.[20] There, local filament density fluctuations resulting in a moderate heterogeneity of the network elasticity were observed at low cross-linker densities. In order to mechanically characterize this weakly cross-linked regime for α-actinin networks, the deformation field of a $R = 0.001$ network is mapped using magnetic tweezer microrheology (see Materials and methods section for details). The deformation field should be sensitive to local heterogeneities in the network elasticity. A magnetic bead is used to create an oscillating deformation using a frequency of 0.5 Hz (red arrows in Fig. 2A). Non-magnetic beads are employed as tracer particles to map the deformation field. Their oscillatory

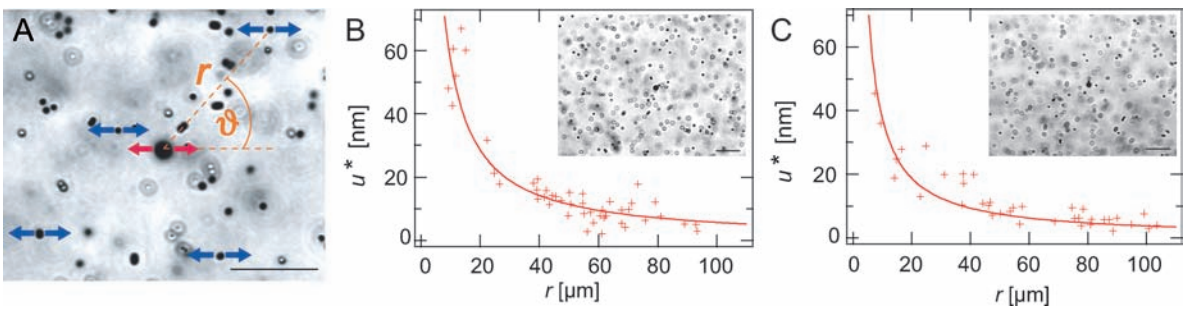

Fig. 2 (A) An oscillating magnetic bead (red arrows) generates a deformation field, which can be detected with tracer particles (blue arrows). The normalized amplitude of the oscillating tracer particles u^* is depicted in (B) and (C) as a function of the distance of the tracer particle from the magnetic bead, r. An entangled solution (B) is compared to a weakly cross-linked α-actinin network ($R = 0.001$) (C). The insets show homogeneous bead distributions that are evaluated to calculate the deformation field. Scale bars denote 20 μm, the actin concentration is 4.75 μM.

motion is tracked and the amplitude $u_{0.5Hz}(r, \vartheta)$ is determined at various sample positions (r, ϑ) (blue arrows in Fig. 2A).

As depicted in Fig. 2B and C, the normalized amplitude $u^*(r) = u(r,\vartheta)/\sqrt{1+3\cos^2(\vartheta)}$ decays with increasing distance r between the tracer particle and the magnetic bead. As indicated by the solid lines, u^* follows the predicted scaling law, $u^* \sim \frac{1}{r}$ (see eqn (2) of the Materials and methods section) for both an entangled actin solution and a weakly cross-linked α-actinin network ($R = 0.001$). This finding shows that in this first mechanical regime no pronounced heterogeneities are present and the network microstructure is still comparable to that of an entangled actin solution.

2. Composite bundle phase

Concomitant with the first mechanical transition at $R = R^*$, the formation of bundles can be observed in confocal microscopy images (Fig. 3A and B) in agreement with former observations.[22] This onset of bundling occurs in a very similar concentration regime as also reported for scruin[9] and fascin,[10] which underlines the generic mechanism of bundle formation in actin networks. In contrast to the purely bundled network formed by fascin, α-actinin creates a heterogeneous, composite phase above the bundling transition: Distinct bundles are embedded in a network that still contains single filament structures (Fig. 3A and B).

This composite phase is similar to the microstructure of actin/scruin networks as reported in ref. 9. Indeed, the roughly quadratic dependence of the plateau modulus (*i.e.* an increase by two orders of magnitude over one decade in R) in this composite regime resembles the scaling relation obtained by Shin *et al.* for scruin networks in the composite phase. As the confocal image depicted in Fig. 3A shows, thick α-actinin/actin bundles are only sparsely present at intermediate α-actinin concentrations. The degree of bundling can be tuned: increasing the nominal α-actinin concentration[22] at a given temperature leads to the formation of thicker bundles and increases the bundle density. Increasing the effective α-actinin concentration by lowering the temperature has the same effect (Fig. 3B). In either case, the resulting network structure retains its heterogeneous character. This suggests that besides the well-defined macromechanical response of the heterogeneous network, the viscoelastic properties could be drastically different on a local length scale.

In order to test this putative difference between the local and macromechanical properties, again a microrheological experiment would be of avail. However, due to the increased stiffness of the network a locally generated deformation decays extremely fast. Given the limited force that can be applied with our magnetic tweezer setup (5 pN), this makes a deformation field mapping as conducted for the weakly cross-linked regime impossible. Instead, the microscopic storage modulus at a given frequency, $G'(0.1\ \mathrm{Hz})$, is determined by active 1-bead magnetic tweezer microrheology and then compared to the macrorheological value. Distributions of this local modulus are obtained by analyzing 80 different bead positions in a given sample for a heterogeneous $R = 0.02$ network (ESI†). The obtained moduli are approximately one order of magnitude lower than the macroscopic result (Fig. 3C); however, the network elasticity can be enhanced by increasing the binding affinity in either case. Moreover, the locally obtained frequency spectrum of such a network resembles the spectrum of a weakly cross-linked network below the cross-link transition.[20] Microrheology probes the mechanical properties of the network on a length scale comparable to the size of the probing particle—in this case 4.5 μm, which is the diameter of the beads used. In the intermediate α-actinin concentration regime the bundle density is still quite low, thus the mechanical fortification caused by the embedded bundles is not detectable on this local scale.

An appropriate parameter to quantify the degree of micromechanical heterogeneity is the relative distribution width $\sigma_{rel} = \sigma / \langle G'(0.1\ \mathrm{Hz})\rangle$ of the local storage moduli.[20] $\langle G'(0.1\ \mathrm{Hz})\rangle$ denotes the average value of the distribution as depicted in Fig. 3C and σ the absolute distribution width. For composite α-actinin networks ($R = 0.02$), this relative distribution width is very low: $\sigma_{rel} \approx 0.22$ for both temperatures investigated and corresponds to values obtained for isotropically cross-linked networks.[20] This further underlines that the observed heterogeneities affect the mechanical properties of the network only on length scales larger than 4.5 μm.

3. Clustered bundle phase

The heterogeneities described so far are still quite modest; on the mesoscopic length scale accessible with classical phase contrast

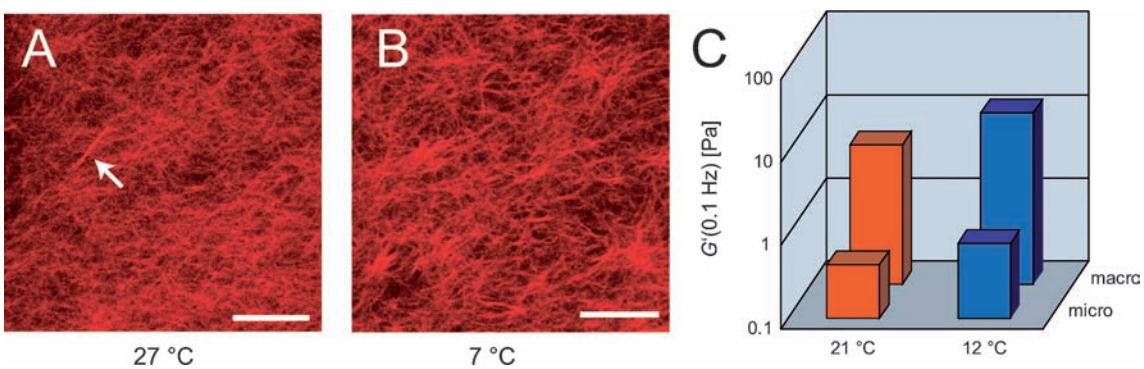

Fig. 3 (A), (B) Confocal micrograph of an composite network ($c_a = 4.75$ μM, $R = 0.05$) where bundles are locally embedded in the network. The degree of bundling can be adjusted by temperature. (A): 27 °C, bundles are very rare (arrow); (B): 7 °C, the degree of bundling is increased but the network structure is still very heterogeneous. Scale bars denote 10 μm. (C): Local and macroscopic elasticity of a composite network ($c_a = 9.5$ μM, $R = 0.02$) at 21 °C (red) and 12 °C (blue).

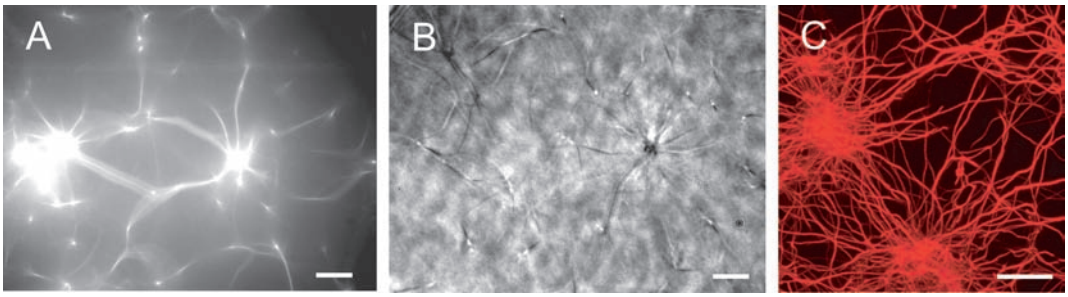

Fig. 4 Epifluorescence (A), phase contrast (B) micrograph of α-actinin networks ($R = 0.5$, $c_a = 2.4$ μM) showing bundle clusters. (C) Z-projection (20 μm) of a confocal micrograph of bundle clusters ($R = 0.5$, $c_a = 4.75$ μM). Pictures are taken at ambient temperature, scale bars denote 10 μm.

microscopy or epifluorescence, individual bundles as detected by confocal microscopy are hardly visible—the bundle diameters are still too small compared to single filaments to stand out from the background network. However, very thick bundles and even stronger heterogeneities in the local network structure should be detectable. Such structural rearrangements occur at higher α-actinin concentrations, $R > R^{\#}$, and can be observed by all kinds of light microscopy techniques as depicted in Fig. 4: star-shaped clusters are detectable both in epifluorescence (Fig. 4A) and phase contrast micrographs (Fig. 4B). Confocal images reveal, that in these clusters lots of bundles, *i.e.* ≈15%, are concentrated in localized spots that have a size of ≈2–20 μm. Interestingly, the star-shaped regions resemble α-actinin/actin foci that are found in living cells where α-actinin and fascin colocalize.[12] Reconstituted actin networks formed by fascin can only reproduce these star-like aggregates if nucleation points are provided, *e.g.* by the Arp2/3 complex.[23] In contrast, α-actinin alone is sufficient to form a network containing clusters of actin bundles. The spatial distribution of these star-shaped bundle clusters can be visualized by a projection of a confocal z-stack at low magnification as depicted in Fig. 5A. In order to determine the fractal dimension d of such bundle clusters, a scaling relation between the cluster mass M and the cluster size R is needed, similar to colloidal aggregates:[24] $M \sim R^d$. The integrated fluorescence intensity of a bundle cluster is proportional to the amount of actin filaments in the cluster and can thus be used to represent M. The determination of cluster sizes from the confocal micrograph is conducted by two methods. First, the cluster is approximated by a sphere and a circular region in the projection is chosen (circles in Fig. 5B). Second, a polygon approximation is applied (squares in Fig. 5B) and the resulting scaling relation is compared to the one obtained by the spherical approximation. Both methods return the identical power law behavior $M \sim R^{1.8\pm0.2}$, which corresponds to a fractal (or Hausdorff) dimension of $d \approx 1.8$. Analyzing the cluster mass distribution reveals a constant distribution for smaller cluster sizes and a decay at higher cluster sizes (see upper inset in Fig. 5B).

However, such regions of clustered bundles are not detectable in our *in vitro* assays at α-actinin concentrations $R < R^{\#}$. Thus, the occurrence of bundle clustering coincides with the mechanical transition point at $R^{\#} \approx 0.1$. This suggests that the lower effectiveness of elasticity enhancement observed for $R > R^{\#}$ is attributable to this type of structural heterogeneity. In order to analyze the effect of local bundle clustering on the mechanical response of bundle networks, we make use of 3-dimensional finite element simulations similar to[25] (for details see the Materials and methods section). A cross-linked network composed of stiff beams ('bundles', each beam is discretized by 11 nodes) with random beam position and orientation (Fig. 6A) is compared to networks with increasing degree of heterogeneity. Networks with one centered cluster of increasing size (Fig. 6B) and networks containing four distinct clusters (Fig. 6C) are investigated. For cluster formation, the beams are merely rearranged to create increasingly heterogeneous network structures. In all cases, the

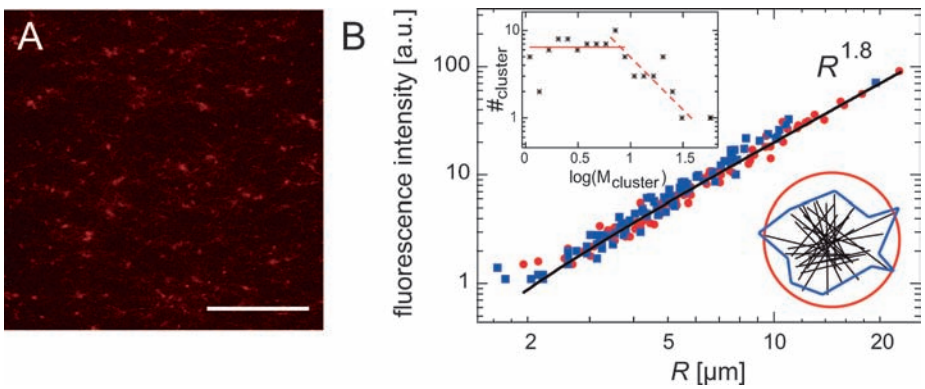

Fig. 5 (A) Confocal micrograph of a bundle cluster network ($c_a = 4.75$ μM, $R = 0.5$) at low magnification (the scale bar represents 100 μm). The picture shows a projection of a z-stack of 150 μm height. (B) The integrated fluorescence intensity of the bundle clusters depicted in (A) is plotted as a function of cluster size, R. Circles denote data points that were obtained by assuming spherical clusters, squares denote a polygon approximation (see lower inset for a schematic). The same power law behavior $\sim R^{1.8}$ is observed by both methods. The upper inset shows the corresponding cluster mass distribution.

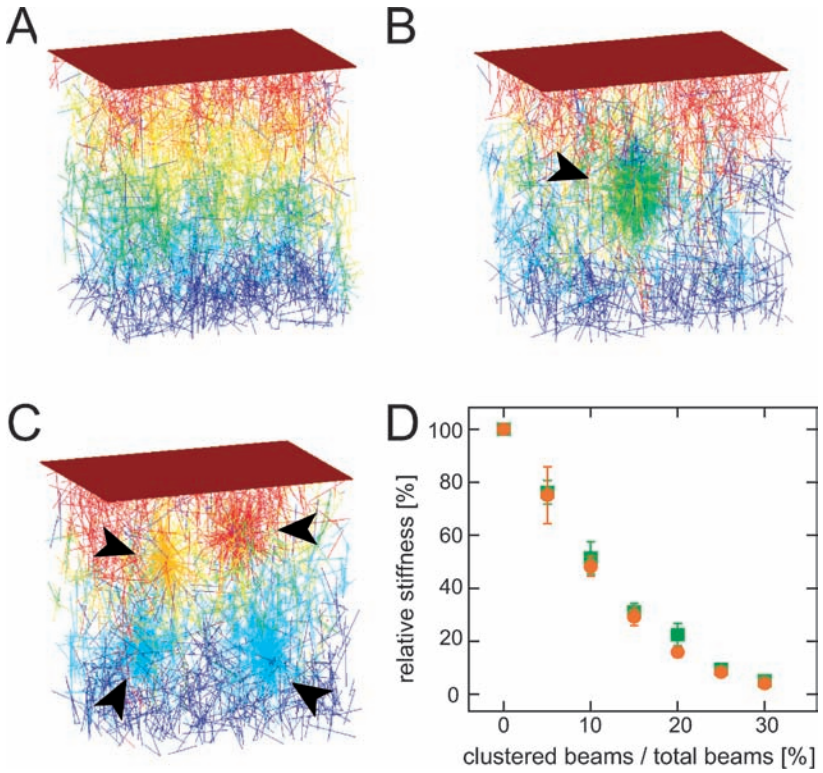

Fig. 6 Finite element simulations of cross-linked bundle networks with increasing degree of heterogeneity: (A) homogeneous network, while 25% of the material is redistributed into one central cluster (B) or four distinct clusters (C). The corresponding network stiffnesses are normalized by the stiffness of the homogeneous network as depicted in (D). The degree of heterogeneity is represented by the ratio of clustered beams to the total number of beams. Circles denote networks with one central cluster, squares denote networks containing four distinct clusters. The total beam density is kept constant throughout all simulations.

total amount of material is preserved. For simplicity, we assume full degree of cross-linking; *i.e.* a cross-link is introduced between each pair of nodes that are closer than 500 nm. It is important to note that the qualitative result of our simulation is largely insensitive towards the detailed assumptions made on the microstructure as shown in the ESI.† As depicted in Fig. 6D, the stiffness of such a network of cross-linked stiff beams decreases roughly exponentially with increasing degree of clustering. The key parameter is the amount of material that is localized in isolated spots as the simulation result is largely insensitive to the number of clusters formed. Note, that clustering drastically affects the network elasticity. Already a degree of heterogeneity of 20%—which roughly corresponds to the amount of clustered bundles under experimental conditions—leads to a drop in the network stiffness by 80%.

Despite the occurrence of bundle clusters, an increase of the network elasticity is observable in our experiments at high α-actinin concentrations—albeit weaker than at intermediate R. Recall that this result is based on increasing R-values. Increasing α-actinin concentrations induce two types of structural rearrangements, that have competing effects on the network elasticity: First, clustering of bundles weakens the network elasticity by concentrating material in localized and isolated spots that are too sparse to allow for percolation of these stiff regions. Second, the bundle density, thickness and stiffness may further increase, which counteracts the increase in average mesh size—similar to what was observed for purely bundled networks.[10] Still, the drastic effect of bundle clustering on the network elasticity observed in the simulations is consistent with the relatively low plateau moduli observed for high α-actinin concentrations ($R > R^{\#}$). If the strong R-dependence valid for intermediate α-actinin concentrations would also extend into the high-R regime, a 30 times higher elasticity would occur for a $R = 0.5$ network.

4. Metastable state of clustered bundles

Pronounced mesoscopic heterogeneities such as bundle clustering are neither reported nor expected for fully equilibrated actin networks. Interestingly, the structural patterns formed and the concomitant mechanical properties are highly reproducible even in this strongly heterogeneous phase of actin/α-actinin networks. Yet the viscoelastic response of a bundle cluster network critically depends on the initial conditions at which the network is formed (Fig. 7A): if an α-actinin network ($R = 0.5$) is polymerized at low temperature only a moderately larger elasticity ($G_0^{\text{initial}}(12\ ^\circ\text{C}) \approx 35$ Pa) is observed compared to polymerization at high temperature ($G_0^{\text{initial}}(21\ ^\circ\text{C}) \approx 20$ Pa). However, if the same 12 °C network is treated by an intermediate heating step to 21 °C a significantly higher plateau modulus, $G_0^{\text{final}}(12\ ^\circ\text{C}) \approx 200$ Pa, is obtained when the network is brought back to its initial temperature. The same final network elasticity $G_0^{\text{final}}(12\ ^\circ\text{C})$ is reached if the sample is polymerized at the high temperature and subsequently cooled to 12 °C. This indicates that the polymerization at 12 °C results in a kinetically trapped

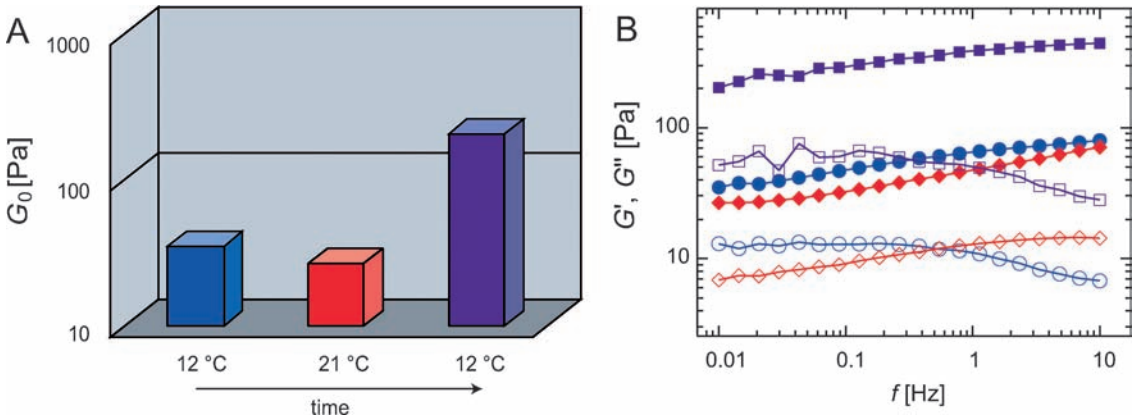

Fig. 7 (A) Plateau modulus G_0 of $R = 0.5$ networks at different temperatures: After polymerization at 12 °C (blue) a heating step up to 21 °C (red) followed by re-cooling to 12 °C (purple) was applied. (B) The frequency spectra corresponding to the plateau moduli shown in (A) are compared directly after polymerization at 12 °C (blue circles), after heating to 21 °C (red diamonds) and after re-cooling to 12 °C (purple squares). Closed symbols denote G', open symbols denote G''.

structure, which can be cured by temporarily lowering the binding affinity of the cross-linking molecules. This is achieved by the transient heating step and allows for a faster spatial equilibration of the cross-linking molecules. Consistently, a very slow increase over $\approx$ 15 h, which saturates at the same high elastic modulus $G_0^{\text{final}}(12\ ^\circ\text{C}) \approx 200$ Pa, is observed for samples that have been polymerized at 12 °C (see ESI†). This phenomenon is not limited to an initial temperature of 12 °C—the network exhibits an identical behavior at higher temperatures (see ESI†). The presented data show that a well-defined final state of the system exists, that is determined by the effective cross-linker concentration—which in turn is set by the temperature-dependent binding affinity of the cross-linking molecule. In all cases, the starting conditions and the subsequent sample treatment dictate how fast this final state is reached. The fractal cluster dimension of $d \approx 1.8$ indicates that this metastable phase is the result of kinetic aggregation and growth effects. The cluster mass distribution obtained here would be consistent with a diffusion limited aggregation process but not with an reaction controlled process underlining the strong interaction potential between actin bundles induced by α-actinin. Still, a quantitative modelling of the complex kinetics which is driving the formation of the network will be necessary in order to rationalize the clustering process in detail: The polymerization and treadmilling of the filaments and the formation of cross-links and bundles occur simultaneously. In addition, the binding of the cross-linking molecules is dynamic with a well-defined off-rate, which—to a certain extent—should also allow for disaggregation. Yet, the clusters themselves are stable and unaffected by the temperature sweeps as confirmed by confocal microscopy (ESI†). This indicates that thermal cross-linker unbinding events between distinct bundles are not sufficient to disaggregate the bundle clusters and local or external forces might be required to rupture the bundle–bundle interconnections.[26]

The thermal curing (Fig. 7) and the retarded temporal equilibration (ESI†) of the system both result in a pronounced change in the viscoelastic spectrum. The frequency spectra of the two low-temperature networks shown in Fig. 7B both exhibit a peak in the loss modulus at low frequencies. This peak in the viscous dissipation is a signature for a transiently cross-linked network: its position is given by the cross-linker off-rate while its height is set by the cross-link density.[6] Unlike the 12 °C data, the spectrum obtained at 21 °C does not show such a low-frequency peak in the viscous dissipation. It rather resembles the featureless shape of frequency spectra obtained for bundled filamin/actin networks,[27] which do not possess point-like cross-links between the bundles. Moreover, after heating and subsequent cooling both components of the viscoelastic frequency spectrum are shifted to higher absolute values while retaining their overall shape. This suggests that the applied temperature cycle (12 °C → 21 °C → 12 °C) leads to an effectively increased interconnectivity: α-actinin molecules that have been trapped in the clustered bundles might be able to escape when their affinity is lowered during the temperature sweep. Clearly, the mechanical properties of cluster networks are highly sensitive on the interconnnectivity, *i.e.* the cross-link density between bundles and clusters (see ESI†). In contrast to this third cross-linker concentration regime ($R > R^{\#}$), where kinetic effects play an important role, networks with $R < R^{\#}$ are virtually unaffected by the starting conditions indicating their thermally well-equilibrated nature (ESI†).

Summary and discussion

We have demonstrated that two types of structural heterogeneities can occur in bundle networks as they are formed by α-actinin. The mechanical behavior of such networks sensitively depends on the binding affinity of the cross-linking molecule. In combination with kinetic trapping effects, this gives rise to a delicate temperature memory of the network elasticity. Temperature changes also lead to alterations in the viscoelastic response of isotropically cross-linked actin networks as they are formed by rigor-HMM. There, the temperature-induced change in the network elasticity can quantitatively be related to the cross-linker density.[7] The structure of an isotropically cross-linked network does not undergo qualitative changes if the temperature is altered—variations in the network elasticity are purely due to changes in the cross-linker distance.[8] However, this

does not hold true for other cross-linked actin networks where multiple structural phases can be reached. In the case of α-actinin, we have shown that 3 distinct structural and therefore mechanical regimes exist. The transition points R^* and $R^\#$ are in good agreement with results obtained from X-ray studies.[15] If such a transition point is crossed due to a variation of the effective cross-linker concentration, drastic structural rearrangements can be triggered which manifest themselves in the elastic network response. As an outstanding example of such a structural rearrangement we have described the formation of fractal bundle clusters. The occurrence of bundle clusters is not limited to the ABP α-actinin, qualititatively similar heterogeneities can be observed for filamin bundle networks, but not for bundle networks formed by scruin,[9] fascin[10] or espin.[28] We speculate, that the size of the ABP is the crucial parameter as long and flexible ABPs like α-actinin or filamin might be required to perform cross-linking and clustering besides bundling.

Materials and methods

Protein and sample preparation

G-actin is obtained from rabbit skeletal muscle following ref. 29, stored and polymerized into filaments as described before.[20] α-Actinin is isolated from turkey gizzard smooth muscle following ref. 30, dialyzed against G-buffer and stored at 4 °C for several weeks. In the experiments the molar ratio R between α-actinin and actin, $R = c_{\alpha\text{-act}}/c_a$, is varied. Polymerization is initiated by adding 10× F-buffer as described in ref. 20. The average length of the actin filaments is controlled to 21 μm using gelsolin[31] which is obtained from bovine plasma serum following ref. 32.

Sample characterization

a. Macrorheology. Approximately 500 μl sample volume is loaded into the rheometer (Physica MCR 301, Anton Paar, Graz, Austria). The viscoelastic response is recorded in the linear regime as described in ref. 20. With the exception of the temperature cycles, samples are polymerized at 18 °C prior to measurements at lower temperature (12 °C). A 30 min waiting time is provided for thermal equilibration.

b. Microrheology and deformation field mapping. A magnetic tweezer microrheometer equipped with phase contrast microscopy is used to obtain local information on the viscoelastic moduli.[33] Distributions of local moduli are obtained as described in ref. 20. For deformation field mapping, monodisperse paramagnetic beads (4.5 μm in diameter, Dynal M-450; Invitrogen, Karlsruhe, Germany) are used to locally deform the network. Non-magnetic polystyrol beads (carboxyl-terminated, 1.2 μm in diameter, Interfacial Dynamics Corp., Portland, USA) are used as tracer particles to determine the deformation field. According to ref. 34, a point force $\boldsymbol{F}$ induces a deformation field $\boldsymbol{u}(\boldsymbol{r})$ in an elastic medium with

$$\boldsymbol{u}(\boldsymbol{r}) = \frac{1+\sigma}{8\pi E(1-\sigma)} \frac{(3-4\sigma)\boldsymbol{F} + \boldsymbol{r}(\hat{r}\boldsymbol{F})}{r} \qquad (1)$$

where σ denotes the Poisson ratio and E denotes the Young's modulus of the material. Using $\sigma = 0.5$ as determined for actin solutions,[35] eqn (1) can be simplified for the two-dimensional case used in this study obtaining

$$u(r,\vartheta) = \frac{3}{16\pi E}\frac{F}{r}\sqrt{1+3\cos^2(\vartheta)} \qquad (2)$$

c. Microscopy. In order to investigate the network structures, actin was labelled with phalloidin-TRITC (Sigma). Epifluorescence and phase contrast pictures were taken with a 63× objective, confocal images were acquired with a confocal microscope (TCS SP5, Leica, Wetzlar, Germany).

Simulations

For simulations of clustered bundle networks, the academic research version of the widely used general-purpose finite element program ANSYS is employed. While recently introduced 3-dimensional simulations of fiber networks[25] are based on Euler–Bernoulli beam elements, we implement Timoshenko beam elements to account for shear deformations within the fibers. A network consisting of 16 000 fibers of equal length $L_F = 50$ μm is restricted to a cube with side length $L_C = 0.5$ mm. The network is confined by rigid plates on the upper and lower boundary. In x- and y-direction free boundaries, *i.e.* zero Neumann boundary conditions are chosen. The lower plate is fixed, contacting fibers are accounted for by zero Dirichlet boundary conditions in the finite element model.

Acknowledgements

This work was supported by Deutsche Forschungsgemeinschaft through Ba2029/8-1, the DFG-Cluster of Excellence Nanosystems Initiative Munich (NIM) and the Munich-Centre for Advanced Photonics (MAP). O. Lieleg acknowledges support from CompInt in the framework of the ENB Bayern. C. Cyron was supported by IGSSE.

References

1 K. E. Kasza, A. C. Rowat, J. Liu, T. E. Angelini, C. P. Brangwynne, G. H. Koenderink and D. A. Weitz, *Curr. Opin. Cell. Biol.*, 2007, **19**, 101.
2 X. Trepat, G. Lenormand and J. J. Fredberg, *Soft Matter*, 2008, **4**, 1750.
3 A. R. Bausch and K. Kroy, *Nature Phys.*, 2006, **2**, 231.
4 B. Wagner, R. Tharmann, I. Haase, M. Fischer and A. R. Bausch, *Proc. Natl Acad. Sci. USA*, 2006, **103**, 13974.
5 D. H. Wachsstock, W. H. Schwarz and T. D. Pollard, *Biophys. J.*, 1994, **66**, 801.
6 O. Lieleg, M. M. A. E. Claessens, Y. Luan and A. R. Bausch, *Phys. Rev. Lett.*, 2008, **101**, 108101.
7 O. Lieleg, K. M. Schmoller, M. M. A. E. Claessens, and A. R. Bausch, 2008, submitted.
8 R. Tharmann, M. M. A. E. Claessens and A. R. Bausch, *Phys. Rev. Lett.*, 2007, **98**, 088103.
9 J. H. Shin, M. L. Gardel, L. Mahadevan, P. Matsudaira and D. A. Weitz, *Proc. Natl Acad. Sci. USA*, 2004, **101**, 9636.
10 O. Lieleg, M. M. A. E. Claessens, C. Heussinger, E. Frey and A. R. Bausch, *Phys. Rev. Lett.*, 2007, **99**, 088102.
11 B. Sjöblom, A. Salmazo and K. Djinovic-Carugo, *Cell. Mol. Life Sci.*, 2008, **65**, 2688.
12 S. Yamashiro-Matsumura and F. Matsumura, *J. Cell Biol.*, 1986, **103**, 631.
13 Y. Tseng and D. Wirtz, *Biophys. J.*, 2001, **81**, 1643.
14 M. M. A. E. Claessens, M. Bathe, E. Frey and A. R. Bausch, *Nature Mat.*, 2006, **5**, 748.

15 O. Pelletier, E. Pokidysheva, L. Hirst, N. Bouxsein, Y. Li and C. Safinya, *Phys. Rev. Lett.*, 2003, **91**(14), 148102.
16 M. Tempel, G. Isenberg and E. Sackmann, *Phys. Rev. E*, 1996, **54**, 1802.
17 I. Borukhov, R. Bruinsma, W. Gelbart and A. Liu, *Proc. Natl Acad. USA*, 2005, **102**, 3673.
18 F. C. MacKintosh, J. Käs and P. A. Janmey, *Phys. Rev. Lett.*, 1995, **75**, 4425.
19 C. Heussinger and E. Frey, *Phys. Rev. Lett.*, 2006, **97**, 105501.
20 Y. Luan, O. Lieleg, B. Wagner and A. R. Bausch, *Biophys. J.*, 2008, **94**, 688693.
21 R. Tharmann, M. M. A. E. Claessens and A. R. Bausch, *Biophys. J.*, 2006, **90**, 2622.
22 P. Bendix, G. Koenderink, D. Cuvelier, Z. Dogic, N. Koeleman, W. Brieher, C. Field, L. Mahadevan and D. Weitz, *Biophys. J.*, 2008, **94**, 31263136.
23 D. Vignjevic, D. Yarar, M. D. Welch, J. Peloquin, T. Svitkina and G. G. Borisy, *J. Cell. Biol.*, 2003, **160**, 951.
24 D. A. Weitz and M. Oliveria, *Phys. Rev. Lett.*, 1984, **52**(16), 1433.
25 E. Huisman, T. van Dillen, P. R. Onck and E. van der Giessen, *Phys. Rev. Lett.*, 2007, 208103.
26 O. Lieleg and A. R. Bausch, *Phys. Rev. Lett.*, 2007, **99**, 158105.
27 K. M. Schmoller, O. Lieleg and A. R. Bausch, *Phys. Rev. Lett.*, 2008, **101**, 118102.
28 K. Purdy, J. Bartles and G. Wong, *Phys. Rev. Lett.*, 2007, **98**, 058105.
29 J. A. Spudich and S. Watt, *J. Biol. Chem.*, 1971, **246**, 4866.
30 S. W. Craig, C. L. Lancashire and J. A. Cooper, *Methods Enzymol.*, 1982, **85**, 316321.
31 P. A. Janmey, J. Peetermans, K. S. Zaner, P. S. Stossel and T. Tanaka, *J. Biol Chem.*, 1986, **261**(18), 8357.
32 H. Kurokawa, W. Fujii, K. Ohmi, T. Sakurai and Y. Nonomura, *Biochem. Biophys. Res. Commun.*, 1990, **168**(2), 451.
33 F. Ziemann, J. Rädler and E. Sackmann, *Biophys. J.*, 1994, **66**, 2210.
34 L. Landau and E. Lifschitz, *Lehrbuch der Theoretischen Physik Band VII: Elastizitätstheorie*, Akademie-Verlag, Berlin, 1975.
35 F. Schmidt, F. Ziemann and E. Sackmann, *Eur. Biophys. J. Biophys*, 1996, **24**, 348.